COMMUNICATION

Atomically Precise Crystalline Materials Based on Kinetically Inert Metal Ions via Reticular Mechanopolymerization

Wen-Yang Gao,[a] Aishanee Sur,[a] Chen-Hao Wang,[a] Gregory R. Lorzing,[b] Alexandra M. Antonio,[b] Garrett A. Taggart, [b] Andrew A. Ezazi,[a] Nattamai Bhuvanesh,[a] Eric D. Bloch,[b] and David C. Powers*[a]

[a] Dr. W.-Y. Gao, A. Sur, C.-H. Wang, A. A. Ezazi, Dr. N. Bhuvanesh, Prof. Dr. D. C. Powers
Department of Chemistry
Texas A&M University
3255 TAMU, College Station, TX 77843, United States
E-mail: powers@chem.tamu.edu

[b] G. R. Lorzing, A. M. Antonio, G. A. Taggart, Prof. Dr. E. D. Bloch
Department of Chemistry and Biochemistry
University of Delaware
Newark, DE 19716, United States

Supporting information for this article is given via a link at the end of the document.

Abstract: Atomistic control of the coordination environment of lattice ions and the distribution of metal sites within crystalline mixed-metal coordination polymers remain significant synthetic challenges. Here we describe the mechanochemical synthesis of a reticular family of crystalline heterobimetallic metal-organic frameworks (MOFs) by polymerization of molecular Ru_2[II,III] complexes, featuring unprotected carboxylic acid substituents, with $Cu(OAc)_2$. The resulting crystalline heterobimetallic MOFs are solid-solutions of Ru_2 and Cu_2 sites housed within $[M_3L_2]$ phases. The developed mechanochemical strategy is modular and allows for systematic control of the primary coordination sphere of the Ru_2 sites within an isoreticular family of materials. We anticipate the reported strategy will provide a rational approach to atomically precise mixed-metal materials.

Reticular synthetic logic, in which systematic perturbation of molecular structures gives rise to predictable variation in materials properties, underpins the rational synthesis of metal-organic frameworks (MOFs).[1] Solvothermal syntheses often yield crystalline materials when metal ions that participate in facile ligand exchange chemistry ($k_{H_2O} > \sim 0.04$ s^{-1} at 298 K[2]) are employed,[3][4] because reversible metal–ligand (M–L) bond formation enables crystallization defects to be annealed (Figure 1a). Under rapid-exchange conditions, synthesis of mixed-metal MOFs typically results in a random distribution of metal sites within the lattice.[5] Incorporation of kinetically inert metal ions as structural elements in crystalline MOFs is a synthetic challenge,[6] and as a result, kinetically inert metal ions, which display slow M–L exchange (i.e. $k_{H_2O} < \sim 0.04$ s^{-1} at 298 K, such as Cr(III), Ru(II or III), Rh(III), Ir(III), and Pt(II)) are rarely encountered in MOFs (Figure 1b). Notable exceptions include Cr(III)-based MIL-100,[7] MIL-101,[8] and $[Ru_6(btc)_4Cl_3]$ (btc = benzene-1,3,5-tricarboxylate),[9] all of which were synthesized at high temperature (≥160 °C), in presence of high concentrations of acid modulators, and obtained only as microcrystalline powders. These observations belie the inherent challenge of crystallization of coordination polymers based on slowly exchanging M–L bonds. Reductive labilization-metathesis strategies have been advanced as an approach to incorporate kinetically inert metal ions,[4] but application of these methods requires that fast ligand exchange kinetics are characteristic of one of the isolable oxidation states of the targeted ions.

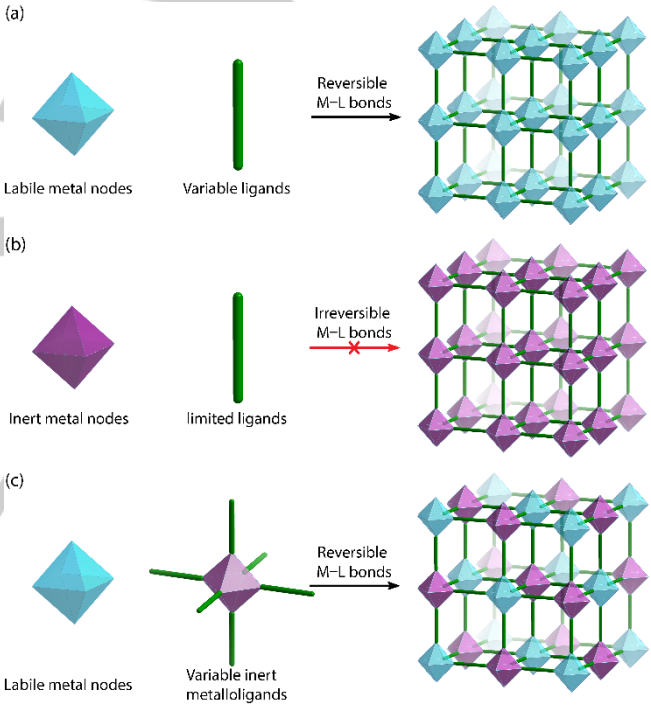

Figure 1. (a) The commonly encountered metal ions in MOFs demonstrate reversible M–L bonds. (b) Kinetically inert metal ions displaying irreversible M–L bonds are rarely encountered in MOFs. (c) A generalized inert metalloligand strategy is demonstrated here for the incorporation of kinetically inert metal ions in MOFs.

Based on the requirement for M–L reversibility to access crystalline materials, the chemical diversity of MOFs is typically limited to rapidly exchanging, weak-field donors, such as carboxylates.[10] Tools that enable systematic variation of the primary coordination sphere of lattice-bound metal ions within isostructural MOF platforms are largely unavailable.[11] These limitations arise because the inherent challenge of incorporating kinetically inert ions is exacerbated for highly basic, strong-field donors, which are commonly encountered in coordination chemistry and catalysis.[12]

As part of our efforts to develop porous catalyst platforms for chemoselective intermolecular C–H amination chemistry, we have been interested in developing modular synthetic methods for Ru_2[II,III]-based MOFs featuring systematically variable primary coordination spheres.[13] Previous efforts, based on metallopolymerization via Sonogashira cross-coupling chemistry, provided amorphous materials.[14] Mechanochemical polymerization has been utilized for the synthesis of MOFs[15] based on Cu_2-[16], Zn_4O-[17], and Zr_6-based[18] metal nodes with organic ligands. We hypothesized that mechanochemical polymerization of kinetically inert metalloligands with metal ions that display facile ligand exchange kinetics would provide access to crystalline heterobimetallic materials in which the distribution of metal sites would be dictated by the sequential synthetic installation (Figure 1c). Here, we report mechanopolymerization of Ru_2[II,III]-based monomers featuring unprotected carboxylic acid substituents to generate a family of isostructural mixed-metal MOFs. The developed method represents a systematic strategy to generate mixed-metal MOFs, in which the metal environment and position are controlled with atomic precision.

We initiated these investigations by developing synthetic chemistry of Ru_2[II,III] complexes (**1**–**3**) featuring free carboxylic acid groups (Figure 2a), which represent molecular building units of a $[M_3btc_2]$ phase. *Bis*-protected ligands **1a** and **2a** were prepared by monodeprotection of the corresponding *tris*-esters (see Supporting Information for details). Thermally promoted ligand exchange between *bis*-esters **1a**–**3a** and $Ru_2(OAc)_4Cl$ or $Ru_2(OPiv)_4Cl$ afforded complexes **1b**–**3b**. Ligand substitution reactions were monitored by electrospray-ionization mass spectrometry (ESI-MS), which provided a value of *m/z* that corresponded to the mass of $[Ru_2L_4]^+$ (**1b** and **2b**) or $[Ru_2L_4Cl]^-$ (**3b**). The ^{1}H NMR spectra of carboxylate- and amidate-based Ru_2L_4Cl (**1b** and **2b**) display similar paramagnetically shifted signals as the non-carboxylated analogues $Ru_2(OBz)_4Cl$ and $Ru_2(HNBz)_4Cl$, respectively. Neither 2-pyridonate-based Ru_2L_4Cl complex **3b** nor the non-carboxylated analogue (compound **S6**, Supporting Information) display well-defined ^{1}H NMR signals when measured in d_6-DMSO at 295 K. Global deprotection, by treatment **1b** with trifluoroacetic acid (TFA) in CH_2Cl_2 or by treatment of **2b** and **3b** with tetrabutylammonium fluoride (TBAF) in THF followed by acidification with HCl, afforded complexes **1**–**3**, which feature free carboxylic acid substituents. In each case, deprotection was monitored by IR spectroscopy. For deprotection of **1b**, disappearance of the C–H bending of the *t*-Bu group (1367 cm^{-1}) was monitored; for **2b** and **3b**, disappearance of the C=O and Si–C stretches (1720 and 840 cm^{-1}) of ester groups were monitored. The formation of **1** and **2** was also monitored by ^{1}NMR spectroscopy.

With access to a suite of Ru_2 complexes featuring carboxylic acid substituents, we investigated mechanopolymerization chemistry to generate porous crystalline materials. We selected $Cu(OAc)_2$ as a co-monomer because it has been commonly employed in mechanochemical syntheses of MOFs[16a, 16b] and displays rapid ligand exchange kinetics.[3a] Ball milling a 1:4 mixture of $Ru_2(H_2btc)_4Cl$ (**1**) and $Cu(OAc)_2{\cdot}H_2O$ in the presence of added MeOH (η = 0.4-0.8 μL/mg,[19] Figure S1) afforded a green-colored crystalline solid that we assign as $[Ru_2Cu_4(btc)_4Cl]$.[20] Powder X-ray diffraction (PXRD) analysis indicates that the obtained material is isostructural to both $[Cu_3(btc)_2]$ and $[Ru_6(btc)_4Cl_3]$ (Figures 3 and S2). For comparison, a series of control experiments were carried out: 1) Milling a mixture of H_3btc and $Ru_2(OAc)_4Cl$ did not afford $[Ru_6(btc)_4Cl_3]$, which is consistent with the aforementioned ligand exchange kinetics at Ru (Figure S3a), and contrasts the ready formation of $[Cu_3(btc)_2]$ upon ball-milling H_3btc and $Cu(OAc)_2{\cdot}H_2O$ (Figures 3 and S2); 2) milling a mixture of $Ru_2(H_2btc)_4Cl$ and MeOH without $Cu(OAc)_2{\cdot}H_2O$ did not generate $[Ru_6(btc)_4Cl_3]$, which further highlights the slow ligand exchange at Ru (Figure S3b); 3) milling a physical mixture of $[Ru_6(btc)_4Cl_3]$ and $[Cu_3(btc)_2]$ (Figure 4a) did not lead to $[Ru_2Cu_4(btc)_4Cl]$ (Figure S4), and 4) pre-formed Cu_2 paddlewheels (*i.e.* $Cu_2(OAc)_4$) appear to be critical for successful mechanochemical synthesis; $[Ru_2Cu_4(btc)_4Cl]$ was not obtained by ball-milling $Ru_2(H_2btc)_4Cl$ and $Cu(NO_3)_2{\cdot}2.5H_2O$ (Figure S5). In addition, attempts to prepare $[Ru_2Cu_4(btc)_4Cl]$ from $Ru_2(H_2btc)_4Cl$ under solvothermal conditions were uniformly unsuccessful.

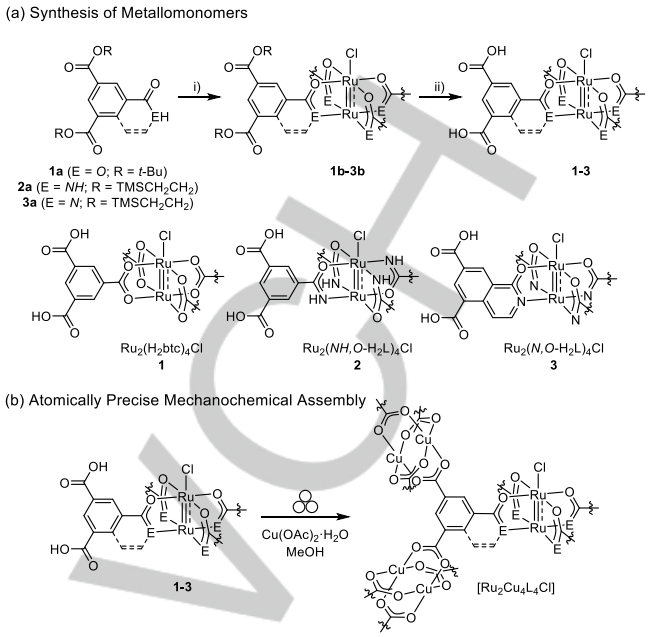

Figure 2. (a) A two-step synthetic procedure, based on ligand exchange followed by global deprotection, to generate metalloligands (**1**–**3**). Conditions: i) **1b**: $Ru_2(OPiv)_4Cl$, PhCl, 90 °C; **2b**: $Ru_2(OAc)_4Cl$, 150 °C; **3b**: $Ru_2(OAc)_4Cl$, PhCl, 150 °C. ii) **1**: TFA, CH_2Cl_2, 23 °C; **2** and **3**: TBAF, THF, 23 °C; 1M HCl, MeOH. (b) Mechanopolymerization of **1**–**3** with $Cu(OAc)_2{\cdot}H_2O$ afforded a family of atomically precise crystalline materials $[Ru_2Cu_4L_4Cl]$ that are isostructural with $[Cu_3(btc)_2]$.

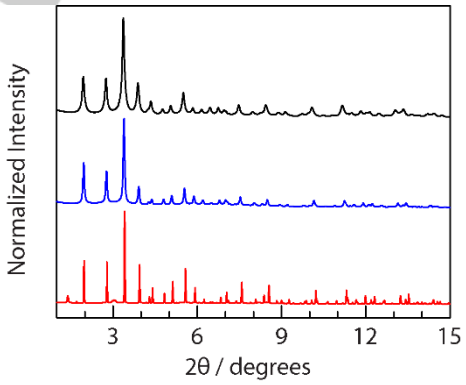

Figure 3. Powder X-ray diffraction (PXRD) patterns of solvothermally generated $[Ru_6(btc)_4Cl_3]$ (—), mechanochemically generated $[Ru_2Cu_4(btc)_4Cl]$ (—), and mechanochemically generated $[Cu_3(btc)_2]$ (—); synchrotron radiation (λ = 0.45411 Å) was employed for these experiments.

The synchrotron PXRD patterns of both $[Cu_3(btc)_2]$ ($a = b = c$ = 26.36724(6) Å, Figure S6a and Table S1) and $[Ru_6(btc)_4Cl_3]$ ($a = b = c$ = 26.7499(9) Å, Figure S6b and Table S1) rwere refined in a $Fm\bar{3}m$ space group, which is in accord with the literature.[9a, 21] Given the kinetic inertness of Ru–O bonds under the mechanochemical conditions, each metalloligand in $[Ru_2Cu_4(btc)_4Cl]$ is expected to be connected to eight Cu paddlewheel nodes (Figure S6c), and each Cu paddlewheel node is expected to be connected to four Cu paddlewheel nodes and four Ru paddlewheel nodes. Such ordering of Ru_2 and Cu_2 paddlewheels would lead to a lower symmetry of $[Ru_2Cu_4(btc)_4Cl]$ as compared to either $[Cu_3(btc)_2]$ or $[Ru_6(btc)_4Cl_3]$.[22] Thus, $[Ru_2Cu_4(btc)_4Cl]$ (Figure S6d) was refined in an $I4/mmm$ space group ($a = b$ = 18.781(7) Å, c = 26.43(1) Å, Table S1). The monotonic lattice contraction from c axis with increasing Cu content (26.7499(9) Å > 26.43(1) Å > 26.36724(6) Å) is consistent with the relative Ru–O (2.02(1) Å in $Ru_2(OAc)_4Cl$) and Cu–O (1.97(2) Å in $Cu(OAc)_2{\cdot}H_2O$) bond lengths.

The metal composition of $[Ru_2Cu_4(btc)_4Cl]$ was investigated by wavelength dispersive spectroscopy (WDS) and by inductively coupled plasma mass spectrometry (ICP-MS) of a nitric-acid-digested sample (Table S2). Both techniques provided a Ru:Cu ratio of 1:2, which is consistent with a high degree of mechanochemical polymerization and the $[Ru_2Cu_4(btc)_4Cl]$ empirical formula. Complementary IR analysis also indicates essentially complete mechanopolymerization (*vide infra*).

X-ray absorption near edge structure (XANES) data for Ru and Cu (Figure S8) suggest that the Ru_2 and Cu_2 units in $[Ru_2Cu_4(btc)_4Cl]$ retain the Ru_2[II,III] and Cu_2[II,II] oxidation states, similar to that of $[Ru_6(btc)_4Cl_3]$ and $[Cu_3(btc)_2]$. Further, Ru K-edge extended X-ray absorption fine structure (EXAFS) data collected for $[Ru_2Cu_4(btc)_4Cl]$ indicate that the local coordination geometry of polymerized Ru_2 sites is unchanged under the mechanochemical synthesis conditions (Figure S9 and Table S3). Specifically, the EXAFS data of $[Ru_2Cu_4(btc)_4Cl]$ collected at the Ru K-edge are consistent with the presence of a Ru environment comprised of four Ru–O distances at 2.03(1) Å, 0.5 (disordered over two axial sites) Ru–Cl distance at 2.40(6) Å, and one Ru–Ru distance at 2.282(9) Å, which is consistent with the molecular structure of $Ru_2(OBz)_4Cl$. Similarly, EXAFS analysis of $[Ru_3(btc)_4Cl_3]$ provided Ru–O: 2.02(1) Å and Ru–Ru: 2.289(5) Å and single-crystal X-ray analysis of $Ru_2(OBz)_4Cl$[23] provided Ru–O: 2.021(4) Å,[24] Ru–Ru: 2.290(1) Å, and Ru–Cl: 2.532(1) Å). Analysis of the Cu-edge data of $[Ru_2Cu_4(btc)_4Cl]$ indicates the presence of four Cu–O vectors at 1.960(5) Å and one Cu–Cu vector at 2.66(2) Å, which is consistent with the Cu_2 structure of the nodes of $[Cu_3(btc)_2]$ (EXAFS: Cu–O: 1.965(7) Å; Cu–Cu: 2.64(2) Å; single-crystal X-ray diffraction: Cu–O: 1.951(4) Å; Cu–Cu: 2.629(1) Å).[21]

IR spectroscopy indicates the presence of discrete Cu_2 and Ru_2 sites in $[Ru_2Cu_4(btc)_4Cl]$ (Figure 4a). The IR spectrum of $[Ru_2Cu_4(btc)_4Cl]$ displays signals at 1447 and 1642 cm^{-1}, which are consistent with COO–Cu_2 stretching frequencies (1443 and 1633 cm^{-1} in $[Cu_3(btc)_2]$[25]). A signal at 1426 cm^{-1} in the IR spectrum of $[Ru_2Cu_4(btc)_4Cl]$ is consistent with a COO–Ru_2 stretching mode and in agreement with the signal at 1432 cm^{-1} observed in $[Ru_6(btc)_4Cl_3]$.[9a, 26] One of the C–COO stretching from the Cu_2 unit (759 cm^{-1} in $[Cu_3(btc)_2]$) was also observed in $[Ru_2Cu_4(btc)_4Cl]$ at 755 cm^{-1}. In addition, IR provides a diagnostic probe for the completeness of the mechanochemical synthesis reaction by examining the disappearance of the carbonyl

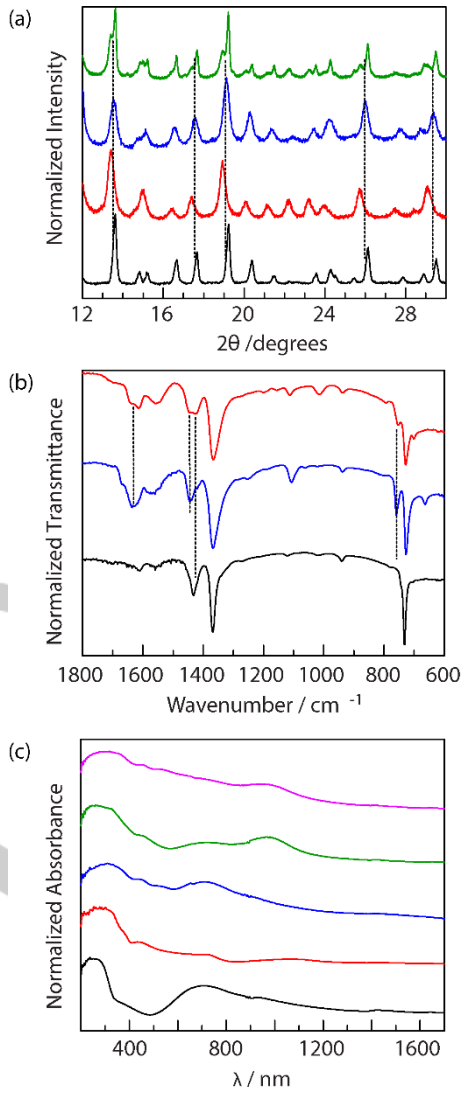

Figure 4. (a) PXRD patterns of $[Cu_3(btc)_2]$ (—), $[Ru_6(btc)_4Cl_3]$ (—), $[Ru_2Cu_4(btc)_4Cl]$ (—), a physical mixture of $[Cu_3(btc)_2]$ and $[Ru_6(btc)_4Cl_3]$ (—). Dotted lines are provided to simplify comparisons with $[Ru_2Cu_4(btc)_4Cl]$, which is distinct from $[Cu_3(btc)_2]$ and $[Ru_6(btc)_4Cl_3]$. (b) IR spectra of $[Ru_6(btc)_4Cl_3]$ (—), $[Cu_3(btc)_2]$ (—), and $[Ru_2Cu_4(btc)_4Cl]$ (—). (c) UV-vis NIR diffusion reflectance spectra of a family of isostructural crystalline $[M_3(btc)_2]$, including $[Cu_3(btc)_2]$ (—), $[Ru_6(btc)_4Cl_3]$ (—), $[Ru_2Cu_4(btc)_4Cl]$ (—), $[Ru_2Cu_4(NH,O\text{-L})_4Cl]$ (—), and $[Ru_2Cu_4(N,O\text{-L})_4Cl]$ (—).

stretching from free carboxylic acid groups at 1725 cm^{-1} (Figure S10b).

Solid-state UV-vis NIR spectra were collected on $[Ru_2Cu_4(btc)_4Cl]$, $[Ru_6(btc)_4Cl_3]$, and $[Cu_3(btc)_2]$ (Figures 4b and S11) and illustrate the co-existence of Cu_2 and Ru_2 in $[Ru_2Cu_4(btc)_4Cl]$. A broad absorption band with λ_{max} centered around 700 nm was observed in both $[Ru_2Cu_4(btc)_4Cl]$ and $[Cu_3(btc)_2]$, which is assigned to the characteristic d-d transitions of the Cu_2 unit. An absorption peak with λ_{max} = 440 nm, assigned as n(O) → π*(Ru_2[II,III]) was observed in both $[Ru_2Cu_4(btc)_4Cl]$ and $[Ru_6(btc)_4Cl_3]$, although the weak intervalence charge transfer band around 1100 nm commonly observed in $Ru(O_2CR)_4Cl$ and $[Ru_6(btc)_4Cl_3]$ was not evident in $[Ru_2Cu_4(btc)_4Cl]$.

Thermogravimetric analysis (TGA, Figure S12) of $[Ru_2Cu_4(btc)_4Cl]$ revealed this material is thermally stable to 200 °C, which is comparable to the thermal stability of $[Ru_6(btc)_4Cl_3]$ (Figure S12). Based on these observations,

$[Ru_2Cu_4(btc)_4Cl]$ was activated by exhaustive methanol exchange followed by heating at 150 °C under vacuum prior to gas sorption analysis. The permanent porosity of $[Ru_2Cu_4(btc)_4Cl]$ was characterized by N_2 adsorption isotherms at 77 K (Figure S13a and Table S4). $[Ru_2Cu_4(btc)_4Cl]$ has a measured Brunauer-Emmett-Teller (BET) surface area of 1051 m^2/g (Langmuir surface area is 1433 m^2/g). In comparison, $[Ru_6(btc)_4Cl_3]$ displays a BET surface area of 958 m^2/g (Langmuir surface area at 1082 m^2/g). The difference in these surface areas is approximately what would be expected based on the difference in empirical formula mass between $[Ru_2Cu_4(btc)_4Cl]$ and $[Ru_6(btc)_4Cl_3]$ (~1.1). Both Ru-based materials display substantially lower surface areas than would be predicted based on the crystal structure (1935 and 1835 m^2/g). The observed surface areas are consistent with both the typical observation than mechanochemically derived materials have lower surface areas than analogous solvothermally prepared materials and the observation that porosity in mechanochemically derived materials is negatively correlated with linker size.[16a] In our synthesis, the "linker" is Ru_2 complex **1**, which is substantially larger than H_3btc. Pore size distribution analysis through density functional theory (DFT) model is summarized in Figure S13b. The observed pores at 6.8 and 8.5 Å are in line with experimental pore sizes of $[Ru_6(btc)_4Cl_3]$ (5.9 and 8.1 Å) and $[Cu_3(btc)_2]$ (8.6 Å). The mechanochemically synthesized $[Ru_2Cu_4(btc)_4Cl]$ displays a broad range of mesopores (20–35 Å), which is consistent with the formation of defects during mechanochemical synthesis.

The developed metallopolymerization provides access to isostructural materials in which the primary coordination sphere of lattice-confined ions is systematically varied. Mechanochemical polymerization of complexes **2** and **3** with $Cu(OAc)_2{\cdot}H_2O$ affords $[Ru_2Cu_4(NH,O\text{-}L)_4Cl]$ and $[Ru_2Cu_4(N,O\text{-}L)_4Cl]$, respectively (Figure 2b). Based on PXRD analysis (Figures S14-S15), the obtained crystalline materials are isostructural to $[Ru_2Cu_4(btc)_4Cl]$ (*i.e.* $[M_3(btc)_2]$ phase). Characterization details for the mechanochemically generated materials (XAS (Figure S16 and Table S5), gas adsorption (Figures S17-S18 and Tables S6-S7), IR (Figures S19-S20), solid-state UV-vis NIR (Figure 4b and Figures S21-S22), and TGA (Figure S23)) are consistent with the indicated empirical formula and indicate the successful incorporation of Ru_2 nodes with systematically varied primary coordination spheres into porous crystalline materials.

In contrast to unsuccessful attempts to prepare $[Ru_2Cu_4(btc)_4Cl]$ by solvothermal methods, solvothermal combination of either $[Ru_2(NH,O\text{-}H_2L)_4Cl]$ or $[Ru_2(N,O\text{-}H_2L)_4Cl]$ — metallomonomers featuring *N,O*-coordination at the Ru_2 site — with $Cu(OAc)_2{\cdot}H_2O$ produced highly crystalline materials (for PXRD, see Figures S14-S15). Solid state UV-vis NIR spectroscopy indicated the incorporation of both Cu_2 and Ru_2 units (Figures S21-S22). The solvothermally generated $[Ru_2Cu_4(NH,O\text{-}L)_4Cl]$ displays a BET surface area of 1580 m^2/g (Figure S17 and Table S6), which is higher than that of the mechanochemically generated sample (418 m^2/g). We hypothesize that $[Ru_2Cu_4(NH,O\text{-}L)_4Cl]$ and $[Ru_2Cu_4(N,O\text{-}L)_4Cl]$ can be accessed solvothermally, while $[Ru_2Cu_4(btc)_4Cl]$ cannot be, due to enhanced stability of the molecular precursors; benzamide and 2-pyridone display are more basic (pK_a = 23.3 and 17.0 in DMSO, respectively) and presumably less easily exchanged from the pre-formed Ru_2 complexes, than that of benzoic acid (pK_a = 11.1).

To evaluate the impact of systematic variation of the primary coordination sphere on the electronic properties of lattice-confined Ru_2 sites, we examined the IR spectra of these materials following impregnation with tetracyanoethylene (TCNE). TCNE was selected as a probe of the local Ru_2 chemical environment because $\nu_{C\equiv N}$ are sensitive to the interactions with transition metal sites.[27] TCNE displays $\nu_{C\equiv N}$ at 2261 and 2228 cm^{-1} (Figure S26). Analysis of samples of $[Ru_2Cu_4L_4Cl]$ materials following exposure to CH_2Cl_2 solutions of TCNE revealed $\nu_{C\equiv N}$ at 2230 and 2204, 2222 and 2200, and 2220 and 2200 cm^{-1} for $[Ru_2Cu_4(btc)_4Cl]$, $[Ru_2Cu_4(NH,O\text{-}L)_4Cl]$, and $[Ru_2Cu_4(N,O\text{-}L)_4Cl]$ (Figure S26), respectively. The systematic shift to lower frequency is attributed to the formation of TCNE adducts of the Ru_2 sites accompanied by fractional charge transfer to the coordinated TCNE ligand from the Ru(II) site (*i.e.* development of $TCNE^{\bullet-}$ character). The extent of π-backbonding, and thus $\nu_{C\equiv N}$ is a reflection of the electron density at the Ru_2 site engaged with TCNE and the order of energies measured for TCNE in $[Ru_2Cu_4(btc)_4Cl]$, $[Ru_2Cu_4(NH,O\text{-}L)_4Cl]$, and $[Ru_2Cu_4(N,O\text{-}L)_4Cl]$ is consistent with the relative donicities of these ligands. Importantly, treatment of an unactivated sample of $[Cu_3(btc)_2]$ with a CH_2Cl_2 solution of TCNE did not result in observable $\nu_{C\equiv N}$ peaks, indicating the lack of adduct formation at the Cu_2 nodes (Figure S27).

In summary, we have developed reticular mechanochemistry that enables synthesis of crystalline materials with atomistic control over both the primary coordination sphere of lattice ions and the connectivity of mixed metal materials. Polymerization is accomplished by reversible Cu–O bond formation between kinetically inert Ru_2-based metalloligands and kinetically labile $Cu(OAc)_2$. The newly obtained crystalline materials are a solid-solution of Ru_2[II,III] and Cu_2 sites in networks that are isomorphous to the related pure Cu_2-based phases. The described mechanopolymerization strategy provides an attractive approach to preparation of mixed-metal MOF materials. Unlike postsynthetic transmetallation or direct solvothermal synthesis under fast-exchange conditions, the described strategy enables synthesis of atomically precise materials under conditions in which no ion scrambling is observed. As such, these materials differ from heterobimetallic materials derived from paddlewheel units that feature two different metal ions[28] in that the current materials are solid solutions of Ru_2 and Cu_2 units. Given the ubiquity of metal paddlewheel building units in MOFs, this strategy complements the current methods of preparing heterobimetallic paddlewheel-based MOFs. This highly modular synthetic strategy allows precise control over the primary coordination sphere of the Ru_2[II,III] sites in solid state materials. This strategy is envisioned to pave an effective avenue to prepare porous MOF materials that feature slow-exchanged inert metal sites and mixed-metal metal nodes with defined environment and positions.

Acknowledgements

This research was supported by the U.S. Department of Energy, Office of Science, Office of Basic Energy Sciences, Catalysis program, under award DE-SC0018977. The authors additionally thank The Welch Foundation (A-1907) for supporting preliminary experimental work. This research used resources of the Advanced Photon Source, a U.S. Department of Energy (DOE) Office of Science User Facility operated for the DOE Office of Science by Argonne National Laboratory under Contract No. DE-

AC02-06CH11357. Synchrotron X-ray diffraction data were collected at Beamline 17-BM of the Advanced Photon Source, Argonne National Laboratory and at Beamline 7-BM of the National Synchrotron Light Source II, a U.S. DOE Office of Science User Facility operated for the DOE Office of Science by Brookhaven National Laboratory under Contract No. DE-SC0012704. We thank Guan-Wen Liu for SEM elemental mapping.

Keywords: reticular chemistry • mechanochemistry • kinetically inert metal • crystalline materials • primary coordination sphere

[1] a) O. M. Yaghi, *J. Am. Chem. Soc.* **2016**, *138*, 15507–15509; b) O. M. Yaghi, M. O'Keeffe, N. W. Ockwig, H. K. Chae, M. Eddaoudi, J. Kim, *Nature* **2003**, *423*, 705–714; c) S. Kitagawa, R. Kitaura, S.-i. Noro, *Angew. Chem.* **2004**, *116*, 2388–2430; *Angew. Chem. Int. Ed.* **2004**, *43*, 2334–2375; d) R. Robson, *Dalton Trans.* **2008**, 5113–5131; e) B. F. Hoskins, R. Robson, *J. Am. Chem. Soc.* **1989**, *111*, 5962–5964; f) B. F. Hoskins, R. Robson, *J. Am. Chem. Soc.* **1990**, *112*, 1546–1554; g) B. Chen, M. Eddaoudi, S. T. Hyde, M. O'Keeffe, O. M. Yaghi, *Science* **2001**, *291*, 1021–1023; h) S. Srivastava, R. Gupta, *CrystEngComm* **2016**, *18*, 9185–9208.

[2] $k_{\mathrm{H_2O}}$ is the rate constant for the exchange of a water ligand from the first coordination sphere on aqua metal ions. The $k_{\mathrm{H_2O}}$ values referred here are at 298 K.

[3] a) D. T. Richens, *Chem. Rev.* **2005**, *105*, 1961–2002; b) L. Helm, A. E. Merbach, *Chem. Rev.* **2005**, *105*, 1923–1960; c) H. Taube, *Chem. Rev.* **1952**, *50*, 69–126.

[4] An arbitary division between inert and labile metal ions was drawn by Taube and was also referenced in Richens' review article.

[5] a) M. Y. Masoomi, A. Morsali, A. Dhakshinamoorthy, H. Garcia, *Angew. Chem.* **2019**, *131*, 15330–15347; *Angew. Chem. Int. Ed.* **2019**, *58*, 15188–15205; b) S. Abednatanzi, P. G. Derakhshandeh, H. Depauw, F.-X. Coudert, H. Vrielinck, P. Van Der Voort, K. Leus, *Chem. Soc. Rev.* **2019**, *48*, 2535–2565; c) G. Ayoub, B. Karadeniz, A. J. Howarth, O. K. Farha, I. Đilović, L. S. Germann, R. E. Dinnebier, K. Užarević, T. Friščić, *Chem. Mater.* **2019**, *31*, 5494–5501; d) W. Guo, W. Xia, K. Cai, Y. Wu, B. Qiu, Z. Liang, C. Qu, R. Zou, *Small* **2017**, *13*, 1702049.

[6] X. Lian, D. Feng, Y.-P. Chen, T.-F. Liu, X. Wang, H.-C. Zhou, *Chem. Sci.* **2015**, *6*, 7044–7048.

[7] G. Férey, C. Serre, C. Mellot-Draznieks, F. Millange, S. Surblé, J. Dutour, I. Margiolaki, *Angew. Chem.* **2004**, *116*, 6456–6461; *Angew. Chem. Int. Ed.* **2004**, *43*, 6296–6301.

[8] G. Férey, C. Mellot-Draznieks, C. Serre, F. Millange, J. Dutour, S. Surblé, I. Margiolaki, *Science* **2005**, *309*, 2040–2042.

[9] a) O. Kozachuk, K. Yusenko, H. Noei, Y. Wang, S. Walleck, T. Glaser, R. A. Fischer, *Chem. Commun.* **2011**, *47*, 8509–8511; b) C. R. Wade, M. Dincă, *Dalton Trans.* **2012**, *41*, 7931–7938.

[10] a) C. H. Hendon, A. J. Rieth, M. D. Korzyński, M. Dincă, *ACS Cent. Sci.* **2017**, *3*, 554–563; b) J. R. Bour, A. M. Wright, X. He, M. Dincă, *Chem. Sci.* **2020**, DOI: 10.1039/c9sc06418d.

[11] For example, to accommodate kinetically inert Cr(III) in MOFs ($[Cr(H_2O)_6]^{3+}$, k_1 (298 K) = 2.4×10^{-6} s^{-1}), two synthetic strategies have been developed: 1) A stepwise reductive labilization-metathesis route which initially reduces Fe(III) to Fe(II), followed by subsequent exchange of Fe(II) to Cr(II) ($[Cr(H_2O)_6]^{2+}$, k_1 (298 K) = ~ 10^9 s^{-1}), and finally oxidization of Cr(II) to Cr(III).[4] Given the slow ligand exchange at Ru(II), the reductive labilization was not judged to be a promising strategy (i.e. $[Ru(H_2O)_6]^{3+}$, k_1 (298 K) = 3.5×10^{-6} s^{-1} and $[Ru(H_2O)_6]^{2+}$, k_1 (298 K) = 1.8×10^{-2} s^{-1}). 2) A synthetic process based on the preparation of a Cr(III) metalloligand featuring free pyridine as a secondary coordination motif that enables additional coordination to a different metal ion, thus achieving extended frameworks. However, this synthetic strategy is restricted to the pyridyl linker as the only secondary coordination motif and $[Cr_3(\mu_3\text{-}O)(CO_2)_6]$ as the only inert metal unit. See a) A. Schoedel, W. Boyette, L. Wojtas, M. Eddaoudi, M. J. Zaworotko, *J. Am. Chem. Soc.* **2013**, *135*, 14016–14019; b) A. Schoedel, A. J. Cairns, Y. Belmabkhout, L. Wojtas, M. Mohamed, Z. Zhang, D. M. Proserpio, M. Eddaoudi, M. J. Zaworotko, *Angew. Chem.* **2013**, *125*, 2974–2977; *Angew. Chem. Int. Ed.* **2013**, *52*, 2902–2905; c) A. Schoedel, L. Wojtas, S. P. Kelley, R. D. Rogers, M. Eddaoudi, M. J. Zaworotko, *Angew. Chem.* **2011**, *123*, 11623–11626; *Angew. Chem. Int. Ed.* **2011**, *50*, 11421–11424; d) Q.-Y. Yang, K.-J. Chen, A. Schoedel, L. Wojtas, J. J. Perry IV, M. J. Zaworotko, *CrystEngComm* **2016**, *18*, 8578–8581.

[12] a) C. Yoo, H. M. Dodge, A. J. M. Miller, *Chem. Commun.* **2019**, *55*, 5047–5059; b) T. A. Jackson, J.-U. Rohde, M. S. Seo, C. V. Sastri, R. DeHont, A. Stubna, T. Ohta, T. Kitagawa, E. Münck, W. Nam, L. Que, Jr., *J. Am. Chem. Soc.* **2008**, *130*, 12394–12407; c) M. E. Crestoni, S. Fornarini, F. Lanucara, *Chem. Eur. J.* **2009**, *15*, 7863–7866; d) J. Annaraj, J. Cho, Y.-M. Lee, S. Y. Kim, R. Latifi, S. P. de Visser, W. Nam, *Angew. Chem.* **2009**, *121*, 4214–4217; *Angew. Chem. Int. Ed.* **2009**, *48*, 4150–4153; e) H. Suzuki, K. Inabe, Y. Shirakawa, N. Umezawa, N. Kato, T. Higuchi, *Inorg. Chem.* **2017**, *56*, 4245–4248.

[13] a) C.-H. Wang, A. Das, W.-Y. Gao, D. C. Powers, *Angew. Chem.* **2018**, *130*, 3738–3743; *Angew. Chem. Int. Ed.* **2018**, *57*, 3676–3681; b) C.-H. Wang, W.-Y. Gao, D. C. Powers, *J. Am. Chem. Soc.* **2019**, *141*, 19203–19207; c) A. Das, J. H. Reibenspies, Y.-S. Chen, D. C. Powers, *J. Am. Chem. Soc.* **2017**, *139*, 2912–2915.

[14] W.-Y. Gao, A. A. Ezazi, C.-H. Wang, J. Moon, C. Abney, J. Wright, D. C. Powers, *Organometallics* **2019**, *38*, 3436–3443.

[15] a) T. Friščić, *Chem. Soc. Rev.* **2012**, *41*, 3493–3510; b) T. Friščić, in *Encyclopedia of Inorganic and Bioinorganic Chemistry*, John Wiley & Sons, Ltd, Chichester, UK, **2014**, pp. 1–19; c) D. Chen, J. Zhao, P. Zhang, S. Dai, *Polyhedron* **2019**, *162*, 59–64; d) T. Friščić, C. Mottillo, H. M. Titi, *Angew. Chem.* **2020**, *131*, 1030–1041; *Angew. Chem. Int. Ed.* **2020**, *59*, 1018–1029; e) W. Yuan, J. O'Connor, S. L. James, *CrystEngComm* **2010**, *12*, 3515–3517; f) X. Ma, W. Yuan, S. E. J. Bell, S. L. James, *Chem. Commun.* **2014**, *50*, 1585–1587; g) S. L. James, C. J. Adams, C. Bolm, D. Braga, P. Collier, T. Friščić, F. Grepioni, K. D. M. Harris, G. Hyett, W. Jones, A. Krebs, J. Mack, L. Maini, A. G. Orpen, I. P. Parkin, W. C. Shearouse, J. W. Steed, D. C. Waddell, *Chem. Soc. Rev.* **2012**, *41*, 413–447.

[16] a) M. Klimakow, P. Klobes, A. F. Thünemann, K. Rademann, F. Emmerling, *Chem. Mater.* **2010**, *22*, 5216–5221; b) M. Klimakow, P. Klobes, K. Rademann, F. Emmerling, *Microporous Mesoporous Mater.* **2012**, *154*, 113–118; c) Y. Chen, H. Wu, Z. Liu, X. Sun, Q. Xia, Z. Li, *Ind. Eng. Chem. Res.* **2018**, *57*, 703–709; d) Z. Nadizadeh, M. R. Naimi-Jamal, L. Panahi, *J. Solid State Chem.* **2018**, *259*, 35–42; e) W. Yuan, A. L. Garay, A. Pichon, R. Clowes, C. D. Wood, A. I. Cooper, S. L. James, *CrystEngComm* **2010**, *12*, 4063–4065.

[17] a) D. Prochowicz, K. Sokolowski, I. Justyniak, A. Kornowicz, D. Fairen-Jimenez, T. Friščić, J. Lewiński, *Chem. Commun.* **2015**, *51*, 4032–4035; b) D. Prochowicz, J. Nawrocki, M. Terlecki, W. Marynowski, J. Lewiński, *Inorg. Chem.* **2018**, *57*, 13437–13442.

[18] a) B. Karadeniz, A. J. Howarth, T. Stolar, T. Islamoglu, I. Dejanović, M. Tireli, M. C. Wasson, S.-Y. Moon, O. K. Farha, T. Friščić, K. Užarević, *ACS Sustainable Chem. Eng.* **2018**, *6*, 15841–15849; b) Y.-H. Huang, W.-S. Lo, Y.-W. Kuo, W.-J. Chen, C.-H. Lin, F.-K. Shieh, *Chem. Commun.* **2017**, *53*, 5818–5821; c) A. M. Fidelli, B. Karadeniz, A. J. Howarth, I. Huskić, L. S. Germann, I. Halasz, M. Etter, S.-Y. Moon, R. E. Dinnebier, V. Stilinović, O. K. Farha, T. Friščić, K. Užarević, *Chem. Commun.* **2018**, *54*, 6999–7002; d) B. Karadeniz, D. Žilić, I. Huskić, L. S. Germann, A. M. Fidelli, S. Muratović, I. Lončarić, M. Etter, R. E. Dinnebier, D. Barišić, N. Cindro, T. Islamoglu, O. K. Farha, T. Friščić, K. Užarević, *J. Am. Chem. Soc.* **2019**, *141*, 19214–19220.

[19] Parameter η (μL/mg) measures the ratio of liquid volume to reactant weight in a liquid-assisted grinding experiment.

[20] Enhanced crystallinity was observed when ball-milling was carried out with MeOH as the additive.

[21] S. S.-Y. Chui, S. M.-F. Lo, J. P. H. Charmant, A. G. Orpen, I. D. Williams, *Science* **1999**, *283*, 1148–1150.

[22] The potential structural order is based on the relative kinetic inertness of Ru–O and Cu–O bonds, confirmed by a series of control synthetic experiments. The microcrystallinity of $[Ru_2Cu_4(btc)_4Cl]$ does not allow for single-crystal X-ray diffraction analysis.

[23] A. Masaaki, S. Yoichi, Y. Tadashi, I. Tasuku, *Bull. Chem. Soc. Jpn.* **1992**, *65*, 1585–1590.

[24] The Ru–O bonds in the crystal structure of $Ru_2(OBz)_4Cl$ are non-equivalent: 2.011(4) and 2.021(4) Å.

[25] T. Toyao, K. Liang, K. Okada, R. Ricco, M. J. Styles, Y. Tokudome, Y. Horiuchi, A. J. Hill, M. Takahashi, M. Matsuoka, P. Falcaro, *Inorgan. Chem. Front.* **2015**, *2*, 434–441.

[26] W. Zhang, M. Kauer, O. Halbherr, K. Epp, P. Guo, M. I. Gonzalez, D. J. Xiao, C. Wiktor, F. X. Llabrés i Xamena, C. Wöll, Y. Wang, M. Muhler, R. A. Fischer, *Chem. Eur. J.* **2016**, *22*, 14297–14307.

[27] a) D. C. Powers, T. Ritter, *Organometallics* **2013**, *32*, 2042–2045; b) P. M. Usov, H. Jiang, H. Chevreau, V. K. Peterson, C. F. Leong, D. M. D'Alessandro, *J. Phys. Chem. C* **2017**, *121*, 26330–26339; c) J. S. Miller, *Angew. Chem.* **2006**, *118*, 2570–2588; *Angew. Chem. Int. Ed.* **2006**, *45*, 2508–2525. d) C. Olson, C. L. Heth, S. H. Lapidus, P. W. Stephens, G. J. Halder, K. Pokhodnya, *J. Chem. Phys.* **2011**, *135*, 024503.

[28] a) J. M. Teo, C. J. Coghlan, J. D. Evans, E. Tsivion, M. Head-Gordon, C. J. Sumby, C. J. Doonan, *Chem. Commun.* **2016**, *52*, 276–279; b) J. Albalad, J. Aríñez-Soriano, J. Vidal-Gancedo, V. Lloveras, J. Juanhuix, I. Imaz, N. Aliaga-Alcalde, D. Maspoch, *Chem. Commun.* **2016**, *52*, 13397–13400; c) M. A. Gotthardt, R. Schoch, S. Wolf, M. Bauer, W. Kleist, *Dalton Trans.* **2015**, *44*, 2052–2056.

Entry for the Table of Contents

Insert graphic for Table of Contents here.

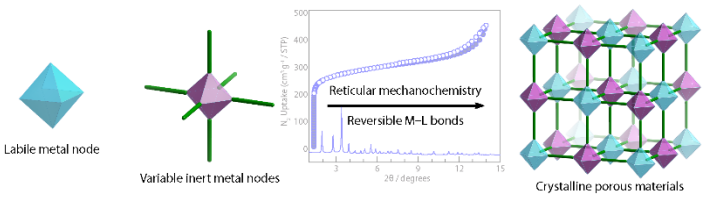

Reticular mechanopolymerization of labile metal nodes and kinetically inert metallomonomers provides a rational synthetic approach to controlling the primary coordination sphere of inert metal nodes and the distribution of metal sites with atomistic precision.

Institute and/or researcher Twitter usernames: @Powers_Lab